Transluminal Pillars - their Origin and Role in the Remodelling of the Zebrafish Caudal Vein Plexus

Helena Roess , Dea Aaldijk , Mykhailo Vladymyrov , Adolfo Odriozola , Valentin Djonov *

Posted Date: 31 August 2023

doi: 10.20944/preprints202308.2080.v1

Keywords: Intussusceptive angiogenesis; caudal vein plexus; transluminal pillar; vessel remodelling

Article

Transluminal Pillars - Their Origin and Role in the Remodelling of the Zebrafish Caudal Vein Plexus

Helena Röss [1], Dea Aaldijk [1], Mykhailo Vladymyrov [2], Adolfo Odriozola [1] and Valentin Djonov [1,*]

[1] Institute of Anatomy, University of Bern, Bern, Switzerland
[2] Theodor Kocher Institute, University of Bern, Bern, Switzerland
* Correspondence: valentin.djonov@unibe.ch; Tel.: +41 31 684 84 32

Abstract: Intussusceptive pillars, regarded as a hallmark of intussusceptive angiogenesis, have been described in developing vasculature of many organs and organisms. The aim of this study was to resolve the question about pillar formation and their further maturation employing zebrafish caudal vein plexus (CVP). The CVP development was monitored by *in vivo* confocal microscopy in high spatio-temporal resolution using the transgenic zebrafish model *Fli1a:eGPF//Gata1:dsRed*. We tracked back the formation of pillars (diameter ≤4µm) and intercapillary meshes (diameter >4µm) and analysed their morphology and behaviour. Transluminal pillars in the CVP arose by a combination of sprouting, lumen expansion, and/or by creation of intraluminal folds, and those mechanisms were not associated directly with blood flow. The follow-up of pillars indicated that one third of them disappeared between 28-48 hours post fertilisation (hpf) and of the remaining ones only 1/17 changed their cross-section area by >50%. The majority of the bigger meshes (39/62) increased their cross-section area by >50%. Plexus simplification and establishment of hierarchy was dominated by the dynamics of intercapillary meshes, which formed mainly by sprouting angiogenesis. These meshes were observed to grow, reshape, and merge with each other. Our observations suggested an alternative view on intussusceptive angiogenesis in the CVP.

Keywords: intussusceptive angiogenesis; caudal vein plexus; transluminal pillar; vessel remodelling

1. Introduction

Intussusceptive angiogenesis (IA), known also as blood vessel splitting, is a complementary mechanism to sprouting angiogenesis (SA) that was proposed for the expansion and remodelling of vascular networks. The hallmarks of IA are thin transluminal pillars with a typical diameter of 1-2.5 µm. They are hypothesized to form by simultaneous invagination of opposing vessel sides, perforation of the contact zone, and finally invasion of perivascular cells and connective tissue fibres (reviewed in [1]). There is abundant evidence for the presence of these thin transluminal structures in developing embryonic vasculature of different species, such as in chicken chorioallantoic membrane (CAM) [2–4], mice embryos [5], human embryos [6], developing frog [7] and most recently in zebrafish embryos [8].

IA may have the following morphological and functional outcomes: (I) Intussusceptive microvascular growth (IMG): insertion of pillars may serve to expand the vascular bed within itself and increase its complexity. Since it requires only a little proliferation rate, this mechanism enables the growth of a plexus with low costs of energy. IMG has been documented in numerous tissues and animal models and is therefore thought to be universal. (II) Intussusceptive arborisation (IAR): pillar arrays may merge and split small arteries and veins to establish hierarchy in the vascular network. (III) Intussusceptive branching remodelling (IBR): pillars may also enable optimisation of the branching geometry by changing the branching angle towards the ideal of a constant level of shear stress with minimal power usage ("Murray's Law"). Hereby, unlike in IMG and IAR, the number of

vessels remains the same or can be reduced by pruning (reviewed in [9]). In line with the findings of IBR, the insertion of transluminal pillars was shown to be flow-dependent and triggered by a local drop in shear stress. This has been demonstrated in vivo [4], in vitro [10] and in computational models [11,12] (reviewed in [13]). IA does not require a remodelling of the surrounding matrix or endothelial cell (EC) proliferation and migration, but the ECs rather increase their size and flatten [14]: it is thus considered to be a more energy efficient process [15]. Therefore, it is not surprising that the intussusceptive pillars have been frequently observed in various types of tumours (reviewed in [16]).

Different mechanisms of pillar formation have been proposed: intraluminal capillary wall fusion [17], capillary wall folding [18] and inverse sprouting [19]. The description of these mechanisms is based on different developmental stages that have been captured on serial semithin or transmission electron microscopy (TEM) images, vascular casts, and with light microscopy images. The currently preferred "intraluminal capillary wall fusion" model proposes four stages of pillar formation: (I) opposite sides of the endothelium make intraluminal processes that contact each other, (II) the endothelial intercellular junctions reorganize and the contact zone is perforated, (III) cytoplasmic extensions of myofibroblasts, pericytes and interstitial fibres infiltrate the pillar, form its core and (IV) merge to create a thin cylindrical pillar, which eventually grows in diameter as it gets penetrated by perivascular cells and extracellular matrix [20]. The alternative "capillary wall folding" mechanism proposes pillar formation by a perforation of a one-sided intraluminal fold [18]. In more detail: first, an intraluminal fold consisting of collagen fibrils and perivascular cell extensions is formed. Next, this fold gets thinner and thinner, until it contains only a bundle of collagen fibrils coated by a single endothelial cell layer (pre-pillar). Finally, the fold is perforated, causing the separation of the pillar. Yet another mechanism termed "inverse sprouting" was proposed much later [19]. According to it, first, a thin transluminal endothelial bridge is formed (how exactly remains open). The endothelial cell then pulls collagen bundles inside this bridge to stabilise it until it stretches throughout the pillar.

Although there are over 200 publications documenting the presence of transluminal pillars in different vessel beds, their development and subsequent growth has, to our knowledge, never been documented in vivo in 3D. Recently, transluminal pillars have also been observed in the caudal vein plexus (CVP) of zebrafish embryos [8]. The transparency of the zebrafish embryonic tissue, the flat morphology, small dimensions of the CVP (ca. 700 x 200 x 50 µm) and the feasibility of in vivo imaging [21] make the CVP an ideal model to address those questions.

The CVP is a transient venous network in the tail of zebrafish, located caudally of the yolk sack extension. It starts forming at 24 hours post fertilisation (hpf) when the heart starts beating and blood creates a simple loop between the dorsal aorta and a caudal vein. The development of the plexus has been described as follows: the starting point is marked by sprouting from the posterior cardinal vein and fusion of neighbouring tip cells. Sprouting from the venous segments in caudal-ventral direction and rapid anastomosis leads to a formation of a primitive plexus by 32-36 hpf ([8,22]). Then, the plexus continues to expand, and hierarchy begins to be established. By 48 hpf the majority of the circulating blood cells is restricted to a vascular loop formed by the dorsal aorta and the most ventral branch of the venous plexus (the caudal vein). The process of gradual elimination of the redundant loops and parallel branches of the plexus further continues until 3 days post fertilisation (dpf) and it retracts in dorso-ventral direction, also due to the tail growing in length. The redundant branches from the central part of the plexus do not fully retract, as observed in pruning, since they serve as a haematopoietic niche [23]. Between 3-5 dpf, some of these connections are observed to drain the blood from the intersegmental vessels to the caudal vein. At 5-7 dpf, the plexus has been simplified to one major loop between the dorsal aorta and the caudal vein [24].

Another question that has not been answered so far concerns the transition from sprouting to intussusception. As documented by various methods in different developing vascular beds, the high number of sprouts during early plexus formation indicates that this phase is dominated by SA (reviewed in [25]). In later stages of the development, the sprout density decreases, and the number and diameter of thin intraluminal pillars gradually increases, which points to the participation of IA in subsequent plexus remodelling. There is, however, no gold standard for the quantification of the involvement of SA versus IA. The semi-quantitative approaches include pillar count versus sprout

 doi:10.20944/preprints202308.2080.v1

count [8, 26], pillar count versus hollow (big meshes) count [27], or the use of endothelial cell proliferation as an indicator of SA and presence of pillars as a marker of IA [28]. Other studies quantify IA based on the pillar count, however, "pillars" may be "small holes" on corrosion casts without specification of the diameter [29], structures of several μm in diameter seen on wild field acquisitions [30, 31], or a circular intraluminal structure [32], a fold [33], an intraluminal contact intermediate of a "pillar" on a histology section [34], or a cross-section acquired by TEM [35]. Many studies use a combination of several methods to describe the wave of IA ([36–39]) but the classification criteria for intussusceptive pillars, when specified at all, are difficult to compare.

To summarise, there is broad evidence for the presence of intraluminal pillars in the developing vascular beds of different species during vessel reorganisation. Nonetheless, little is known about the mechanisms of the formation and subsequent growth of pillars and intercapillary meshes. Zebrafish embryos present a valuable and well-documented model for angiogenesis research with the possibility of in vivo imaging (reviewed in [40]), we have chosen the zebrafish CVP to document the mechanisms of pillar formation. Our aim was to gain insight into the role of pillars in plexus expansion and remodelling in high spatio-temporal resolution.

2. Results

2.1. Appearance, morphology and distribution of pillars in the developing CVP

Previous data suggest that the CVP develops between 30-42 hpf, mainly by IA in proximal perfused regions and by continuing SA in distal non-perfused regions [8]. In line with that, we observed numerous transluminal pillars present in the CVP during that time.

At 48 hpf, the caudal vein plexus consisted of a single artery and a venous plexus, which originally had a honeycomb-like pattern (Figure 1 (a) i). Short vessel segments encircled the intercapillary meshes (rectangles, Figure 1 (a) ii), and further complexity was added to the plexus by thin intraluminal pillars (circles, Figure 1 (a) ii). Most pillars were found in the venous part of the CVP, rather along the plexus border than in the centre, and these pillars were perpendicular to the plane of blood flow (Figure 1 (a) iii, iv). Occasionally, a pillar was present in the most caudal part of the dorsal artery, close to where it made a loop towards the caudal vein. Such pillars had a flat angle to the body symmetry plane and were longer than the vessel diameter.

In in vivo confocal scans, meshes had a sand-clock or biconcave profile (Figure 1 (a) v to viii), while pillars appeared as straight cylindrical structures (Figure 1 (a) ix to xii) and furthermore showed typical morphology on TEM (data not shown). The average pillar diameter was 1.7±0.7 μm and they had an average height of 11±4.6 μm (Figure 1 (b), n=67, measured at 48 hpf).

The pillar count per plexus reached its maximum around 36-48 hpf. From 3 dpf (72 hpf) onwards, there was a highly significant reduction in the pillar number. Note the very high biological variability of pillar numbers and the persistence of many pillars even until 4 dpf (96 hpf) (Figure 1 (c)) and likely onwards, although plexus remodelling had been mostly completed by that time.

Preprints (www.preprints.org) | NOT PEER-REVIEWED | Posted: 31 August 2023 doi:10.20944/preprints202308.2080.v1

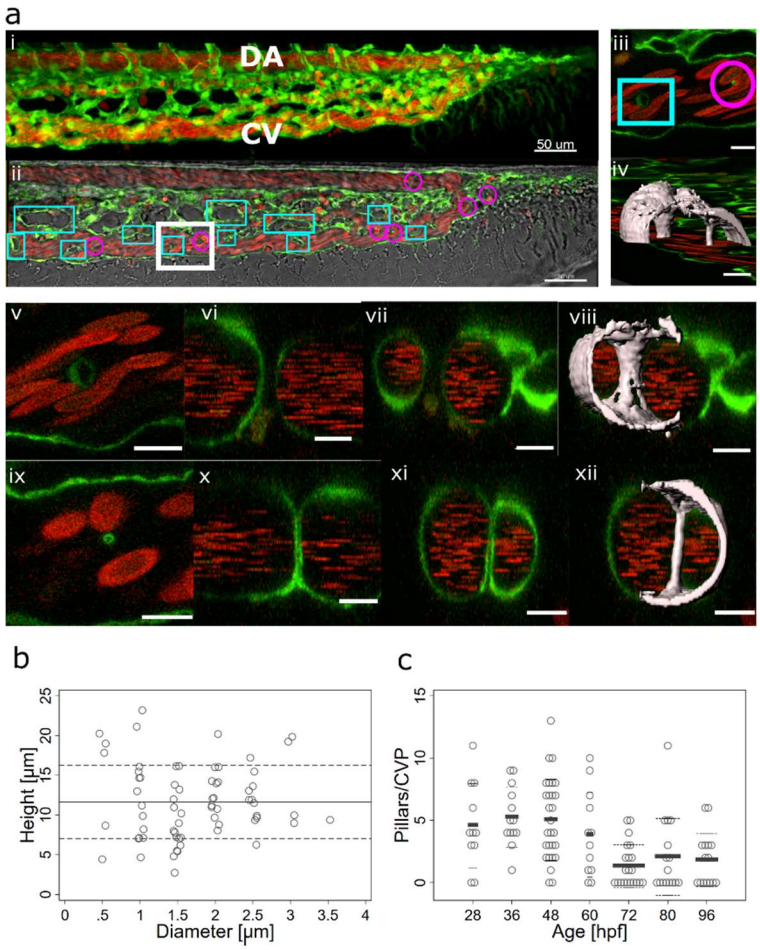

Figure 1. Morphology of pillars and meshes and pillar count per plexus. (a) Confocal images of Fli1a:eGFP//Gata1:dsRed embryos, endothelium in green (eGFP), erythrocytes in red (dsRed), the wide field channel is in greytones. I, II: Overview of the CVP at 48 hpf shows the blood flow in the dorsal aorta and the caudal vein (DA, CV), the tail of the fish is pointing to the right of the image. I is a maximum intensity projection of Z-stacks, II a single slice image. Cyan rectangles show meshes, magenta circles pillars within the plexus, the region indicated by a white rectangle is shown in detail in III (single slice) and IV (3D reconstruction of the endothelium based on the confocal data). The orientation of the pillar is perpendicular to the blood flow (moving erythrocytes seen as red streaks). V, VI, VII and VIII show further details of the small mesh from image III, in V a cross section (xy), in VI and VII a longitudinal section (yz and xz, perivascular cells infiltrating the mesh are apparent) and in VIII the 3D reconstruction in grey. In IX, X, XI and XII details of the pillar from image III are seen, in IX a cross section (xy), X and XI a longitudinal section (yz and xz) and in XII the 3D reconstruction in grey. Note the different shape and diameter of the mesh in comparison to the pillar. Scale bar I and II: 50 µm, other images: 10 µm; (b) Distribution of pillar height (length in z-axis) and diameter (in xy plane) at 48 hpf. The thick line represents the average height, dashed lines the correspondent standard deviation; (c) Number of pillars per plexus measured in in vivo confocal images between 28 and 96 hpf (1 and 4 dpf). Thick lines represent the average pillar number for each time point, thin dashed lines the correspondent standard deviation.

2.2. Mechanisms of pillar formation

To investigate how these pillars formed, we imaged the developing CVP using time-lapse confocal microscopy from the end of the sprouting phase, during the whole intussusceptive phase, and beyond (between 30-48 hpf). Then we tracked 74 pillars (defined by their morphology at 48 hpf) up to 16 hours back in time. What we could observe were three main processes behind the pillar formation: (1) interaction of filopodia and tiny sprouts with each other and (2) lumen formation or (3) lumen expansion.

Preprints (www.preprints.org) | NOT PEER-REVIEWED | Posted: 31 August 2023 doi:10.20944/preprints202308.2080.v1

The common precursor of pillar formation was an intraluminal fold, whose perfusion led to a creation of a pillar. If it formed from an assembly of endothelial cells during lumen formation, we spoke of lumen expansion (LE, Figure 2) as the major force. If the intraluminal fold arose by merging of tiny sprouts from a lumenised vessel segment, the predominant mechanism was sprouting angiogenesis (SA, magenta arrows, Figure 3). And finally, if the intraluminal fold arose from a vessel without the apparent participation of sprouts, we borrowed the term capillary wall folding (CWF, Figure 4) (the driving force seemed to be the growth of the vessel diameter but a barrier outside the vessel stood in the way) because it resembled the mechanism proposed by Patan et al [18].

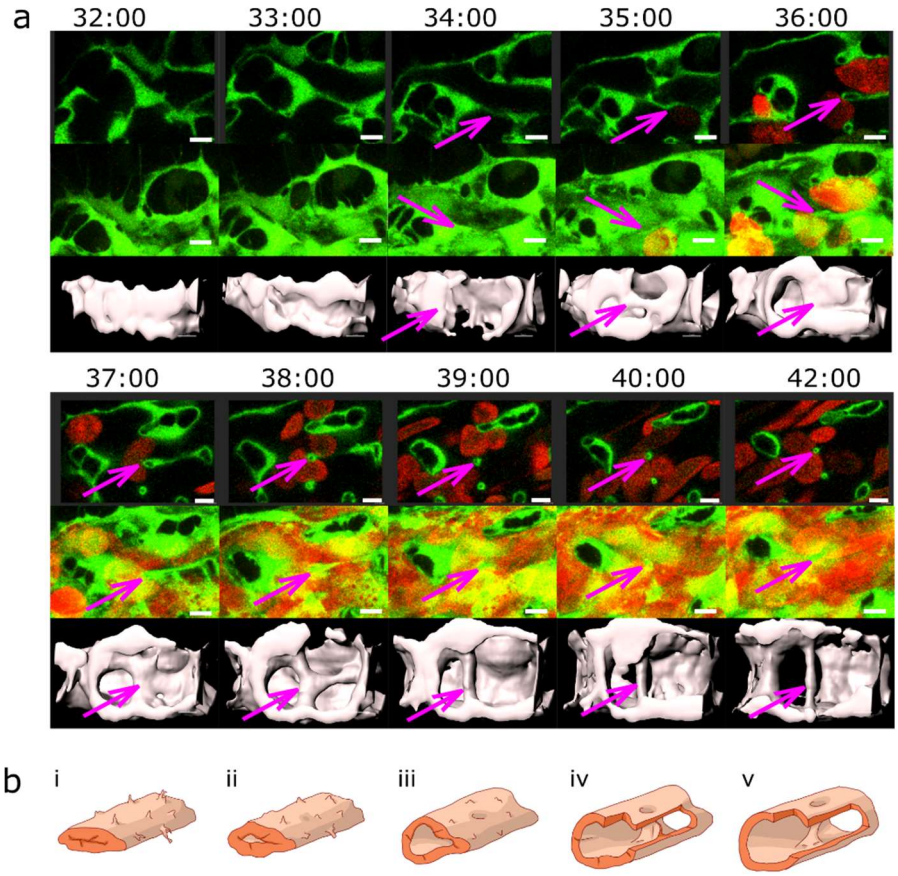

Figure 2. Lumen expansion and pillar formation.(a) Confocal images showing the formation of a pillar by lumen expansion. The pillar is marked with a magenta arrow. The example shows the high plasticity of the developing endothelial network. The pillar starts being visible in the 3D reconstruction at time point 35:00 and in the single slice at time point 36:00. As the pillar forms, weak connections to the endothelial walls (endothelial bridges) may be apparent, as seen in the 3D reconstruction at time point 38:00 but they get thinner and break soon (time point 39:00). First row: one confocal section of 1µm, endothelium in green (eGFP), erythrocytes in red (dsRed). Second row: maximum intensity projection. Third row: 3D reconstruction showing surface models of the endothelium in grey (based on the GFP channel). Time points (hh:mm post fertilisation) are valid for each column. Scale bars: 5 µm. (b) Illustration of the proposed mechanism.

Preprints (www.preprints.org) | NOT PEER-REVIEWED | Posted: 31 August 2023 doi:10.20944/preprints202308.2080.v1

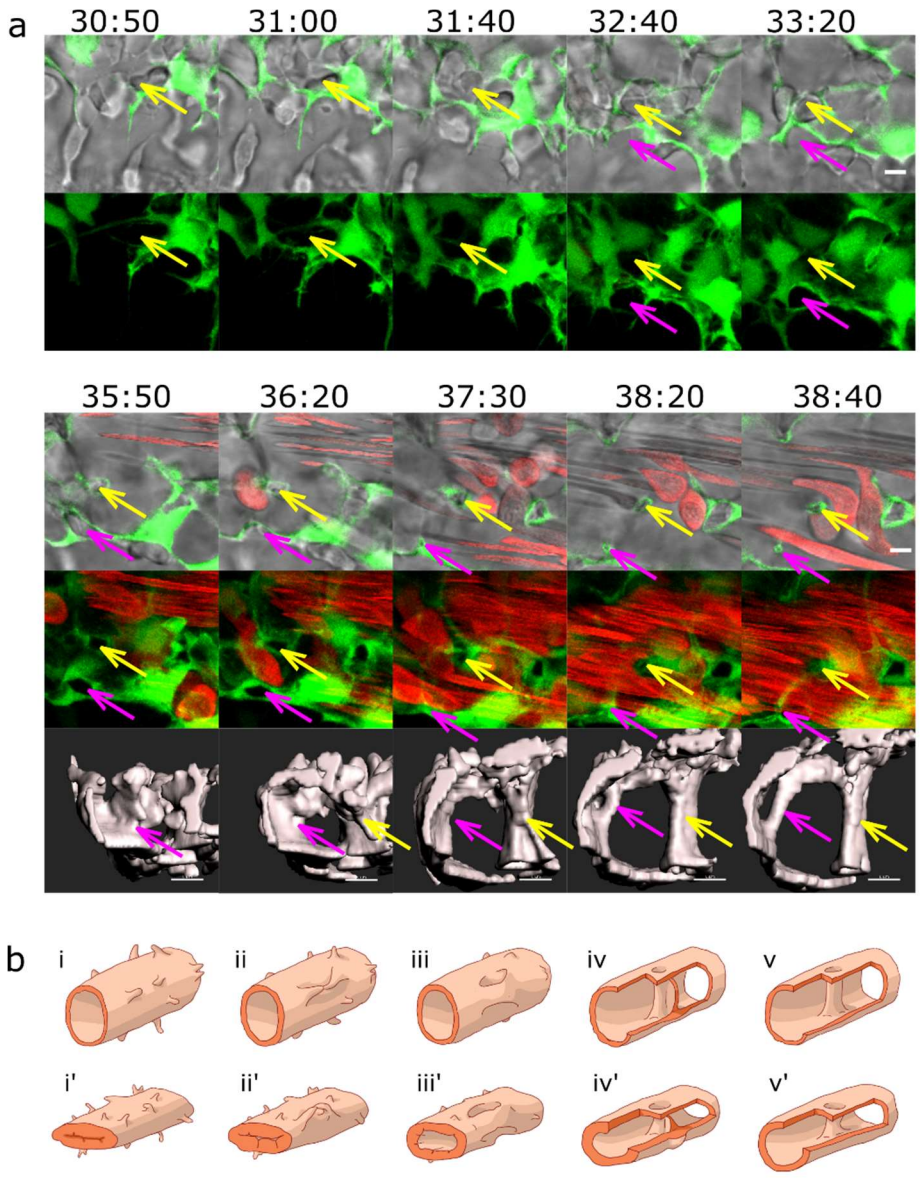

Figure 3. Pillar formation by fusion of sprouts.(a) Confocal images showing the formation of two pillars (indicated by coloured arrows) that could be tracked back to sprouting angiogenesis. First, endothelial cells form highly dynamic filopodia that make transient contacts (time point 30:50 and 31:00). Second, they form small loops that are not perfused first, visible at time point 32:40 (yellow arrow) and 33:20 (magenta arrow). This stage corresponds to the "intraluminal fold", except that the lumen is very narrow and not well defined yet. Third, vessel perfusion starts: the lumen expands and the pillar detaches from the vessel wall. This can be seen at the time points 37:30 – 38:40 (magenta arrow). The pillars grow in z-axis (usually perpendicular to the plane of the CVP) and the pillar diameter often shrinks. The structure is morphologically visible as a pillar only now. Endothelium in green (eGFP), erythrocytes in red (dsRed). First row: single slice of 1 µm with bright field channel added. Second row: maximum intensity projection. Third row: 3D reconstruction in grey. All confocal images are in the same magnification. Time points (hh:mm post fertilisation) are valid for every three (two) representations below. Scale bar: 5 µm. (b) illustration of the proposed mechanisms, i-v: sprouting (corresponding to the pillar marked by the magenta arrow), i'-v': combination of SA and LE (corresponding to the pillar marked by the yellow arrow).

Preprints (www.preprints.org) | NOT PEER-REVIEWED | Posted: 31 August 2023 doi:10.20944/preprints202308.2080.v1

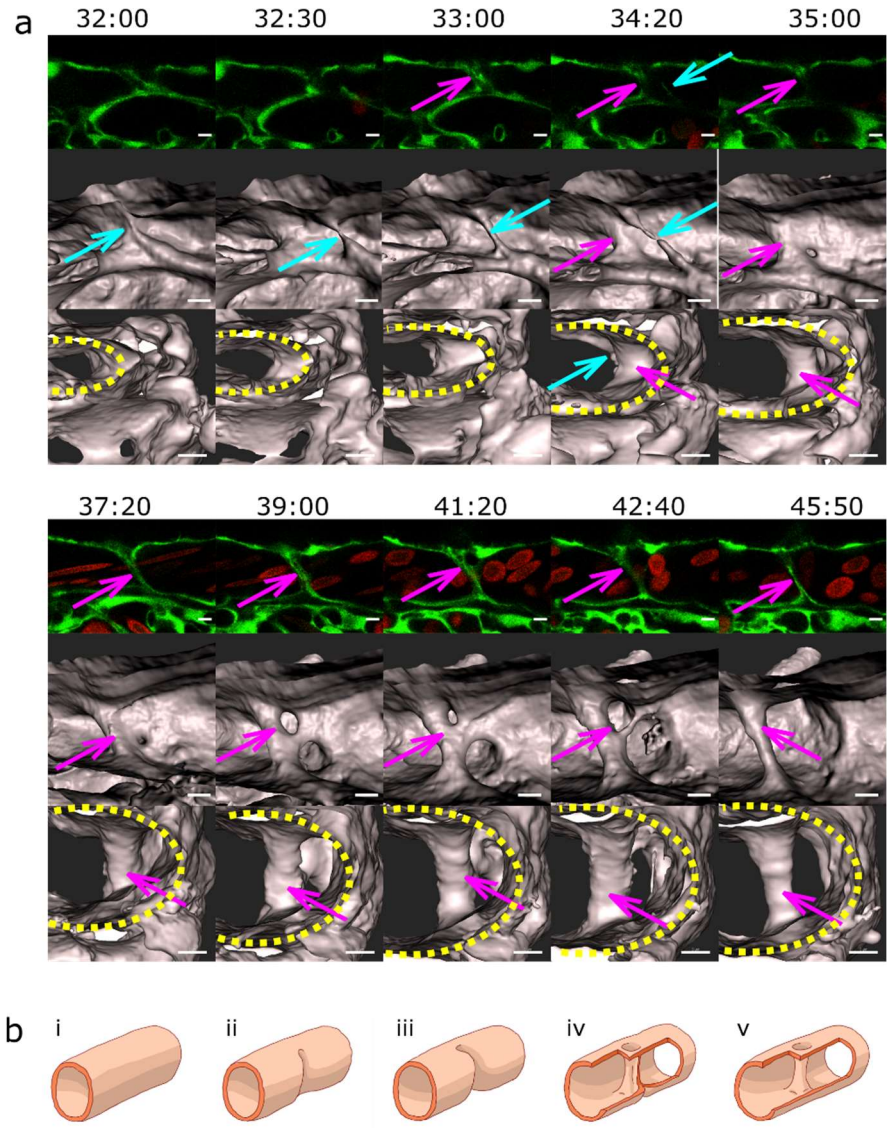

Figure 4. Pillar formation by capillary wall folding.(a) Development of one of the strong transversal pillars that are frequently observed in the caudal part of the dorsal aorta (DA). The pillar starts to form as an intraluminal fold (time point 34:20, magenta arrow) and grows as the lumen of the DA expands. Briefly, another thin pillar (cyan arrows) or endothelial bridge forms by the same mechanism (time points 32:00-33:00) but gets thinner and ruptures soon afterwards (34:20). First row: one confocal section of 1µm, endothelium in green (eGFP), erythrocytes in red (dsRed). Second row: maximum intensity projection of the same region. Third and fourth row: surface models of the endothelium in 3D (based on the GFP channel) in two different perspectives, the yellow dotted line shows the lumen of the dorsal aorta. Time points (hh:mm post fertilisation) are valid for each column. Scale bars: 5 µm. (b) Illustration of the proposed mechanism based on the 3D reconstructions above.

Most pillars formed by a combination of SA and LE (yellow arrows, Figure 3) or by a mixture between SA and CWF, but sometimes one of them seemed to be dominating over the others, as seen in the selected examples. These processes were reversible and sometimes the intraluminal fold was smoothened again, without a pillar being formed. Even an already formed pillar could retract back to a capillary wall fold and eventually fully disappear.

We also observed thin "pillars" reminiscent of endothelial bridges documented by Paku et al. [19] (Figure 2 and 4). Endothelial bridges, as the name suggests, consist only of endothelial cell connections spanning through the lumen, with no visible 'core', and they emerge from the luminal side of endothelial cells. However, these fragile connections were very unstable, got thinner und broke within an hour or two.

Preprints (www.preprints.org) | NOT PEER-REVIEWED | Posted: 31 August 2023 doi:10.20944/preprints202308.2080.v1

2.3. Blood flow and pillar formation

According to literature, major stimuli for pillar formation (whether by intraluminal invagination or by the alternative mechanism) are steep changes in blood flow and shear stress. We analysed Fli:eGFP//sih embryos completely lacking blood flow and thus with no local shear stress differences (Figure 5 (a) i and ii). Before the onset of circulation (24-26 hpf), the vasculature of silent heart (sih) embryos resembled that of wild type (wt) siblings (data not shown, in agreement with [41]), but at 48 hpf, there was no vascular network formed: the venous part was inflated and filled with blood cells, and there were numerous thin pillars in the lumen. The main mechanism of pillar formation is fusion of sprouts, alone or in combination with lumen expansion, which are the mechanisms seen in wt embryos too (Figure 5 (b)). So, even though pillars were present in sih embryos, they did not contribute to the development of a functional vessel network.

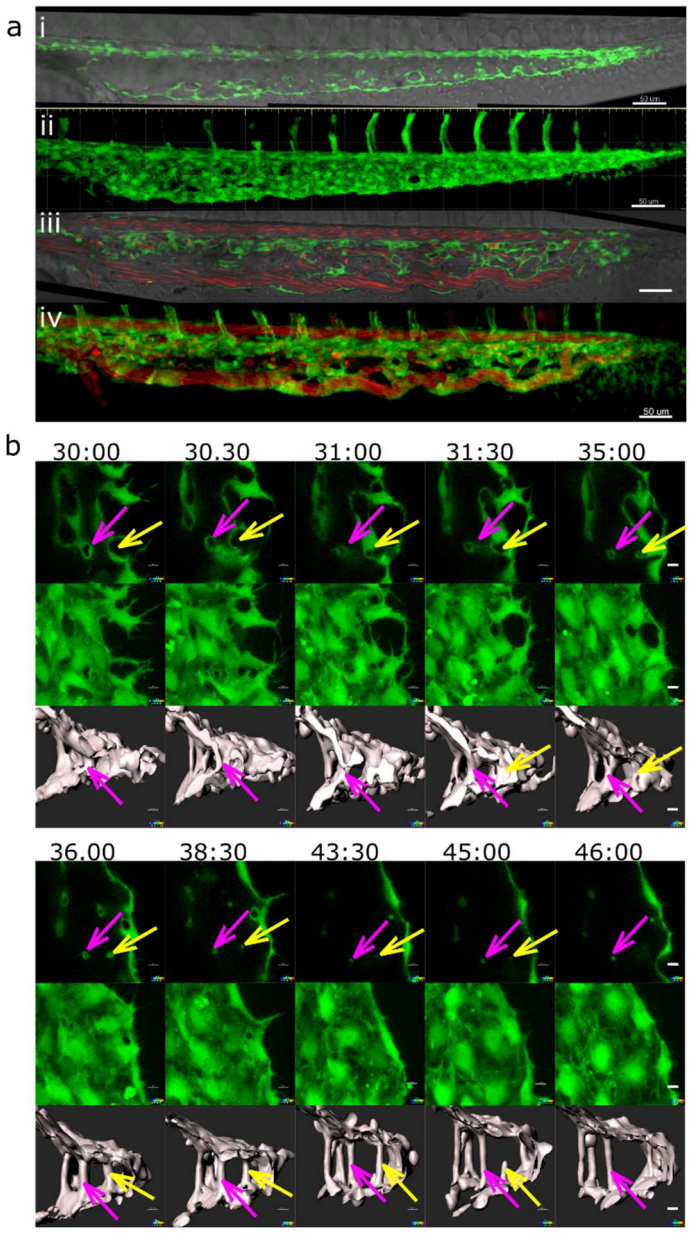

Figure 5. Pillar and mesh formation in the absence of blood flow. a: CVP of a Fli:eGFP//sih embryo (I and II) compared to the CVP of a wt embryo (III and IV) at 48hpf. The sih embryo does not have any blood flow and thus no local shear stress differences. I and III: single confocal section, II and IV: maximum intensity projection. Endothelium in green (eGFP), erythrocytes in red (dsRed), and bright field in grey (I and III). Note that there are frequent pillars (visible as tiny circles in single confocal

Preprints (www.preprints.org) | NOT PEER-REVIEWED | Posted: 31 August 2023 doi:10.20944/preprints202308.2080.v1

sections) but very few meshes (oval-like shapes, corresponding to dark spots in II). This stands in contrast to the wt CVP seen in III and IV, where there are only a few pillars visible. Scale bars: 50 µm. b: Mechanism of pillar formation in the absence of blood flow. The driving forces of pillar formation in Fli:eGFP//sih embryos are sprouting and lumen expansion, i.e. the same phenomena as in wt embryos. The development of two pillars is marked by coloured arrows, one of them disappears at the end of the image sequence (time point 45:00-46:00, yellow arrow). First row: one confocal section. Second row: maximum intensity projection of the same region. Third row: surface models of the endothelium in grey (based on the GFP channel). Time points (hh:mm post fertilisation) are valid for each column. Scale bars: 5 µm.

This demonstrated that pillar formation by fusion of sprouts does not require blood flow, which is in agreement with the fact that sprouts can arise from unperfused vessels.

2.4. Further fate of pillars and intercapillary meshes

Previous studies linked pillars to vascular splitting: small pillars are thought to expand and evolve into meshes, and pillars or meshes in an array may fuse with each other to form a longitudinal slit. We investigated in vivo whether the pillar or mesh cross-section areas increased in time, and whether serried pillars or meshes merged with each other.

The cross-section area of meshes and pillar has been measured at time point 28-32 hpf and again at 44-48 hpf, calculated the absolute area change, and plotted it against the cross-section area at the first time point (Figure 6 (a)). There was a positive correlation between pillar/mesh size and its growth (black rectangles), and also between its size and its diminishment (grey rectangles). The bigger the structure, the bigger was the absolute change in its area over time.

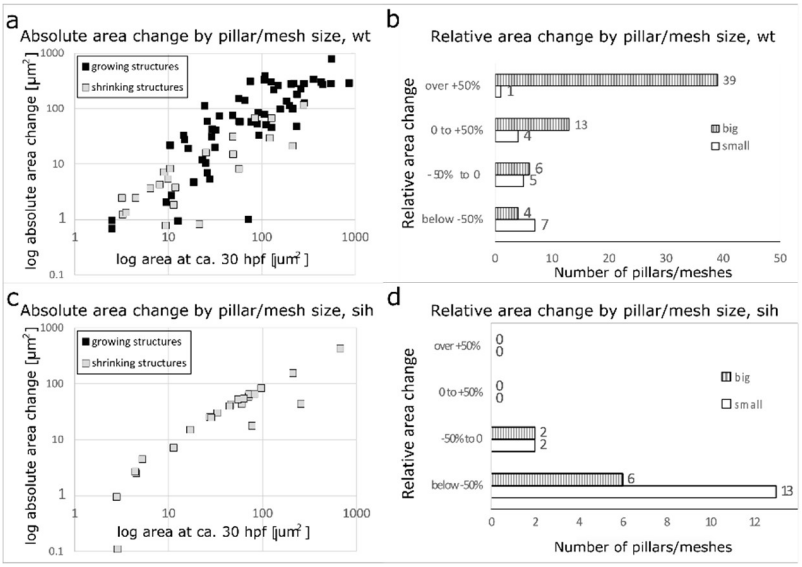

Figure 6. Absolute and relative change in mesh/pillar area depending on their initial size and the presence or absence of blood flow. (a, b) : wt embryos. (c,d): sih embryos (no blood circulation). Changes in pillar/mesh size at 44-48 hpf are plotted against their initial area at 28-32hpf. In wt (a), the bigger the mesh, the more it usually grew or shrank, while in sih (c), all measured meshes shrank independently from their initial size. Relative changes in pillar/mesh area are seen in (b, d): In wt, very small meshes and pillars with an area <12 µm2 at 28-32 hpf (corresponding to a diameter below 4 µm, white bars in the tables) did not grow or shrink much, while the majority of bigger meshes (>12 µm2, striped bars) changed their size (b). In sih, all the structures shrank, independently from their initial size (d).

We further plotted the count of pillars/meshes against the relative area change (Figure 6 (b)). Only 1 out of 17 pillars (or very small meshes, area below 12.5 µm², corresponding to a diameter of 4

Preprints (www.preprints.org) | NOT PEER-REVIEWED | Posted: 31 August 2023 doi:10.20944/preprints202308.2080.v1

μm or less, n=17) changed its cross-section area by more than +50%. The average relative cross-section area change was -16±68% (absolute average change +1.1±9.9 μm²).

In contrast, the majority of meshes (area over 12.5 μm², n=62) increased their area by more than +50% over time (39 out of 62 meshes). The average relative difference in the cross-section area of meshes between the two time points was +95±110% (absolute average change +112±150 μm²).

The increase in mesh area was flow-dependent: all the meshes and pillars in sih embryos decrease their cross-section area over time (Figure 6 c, d).

2.5. Merging of adjacent pillars/meshes

Of 78 pillars that were observed between 28-32 hpf, two thirds (n=52) remained present even at 48 hpf. One third of the pillars (n=26) disappeared between 32-48 hpf, either by merging with a vessel wall or a nearby mesh (n=17, more frequently with an outer vessel branch than with an inner mesh) (Figure 7 (c,d)) by a process that resembled reversed "capillary wall folding" and led to the disappearance of the barrier to blood flow. Since there was no observable increase in the mesh diameter after it had fused with the pillar, it appeared that this process did not contribute to vessel splitting.

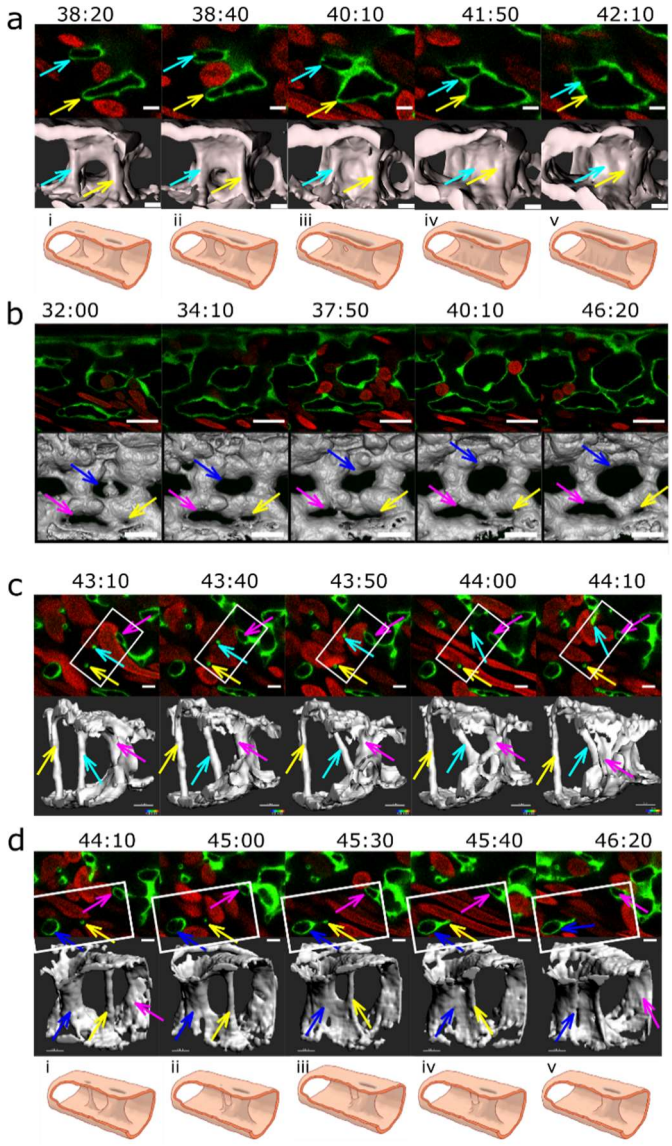

Figure 7. Vascular splitting by merging of meshes; pillar disappearance by merging with a mesh (capillary wall folding reversed). Different examples of pillar and mesh behaviour seen in confocal

images. Endothelium in green (eGFP), erythrocytes in red (dsRed). First row: single slice. Second row: 3D reconstruction of the endothelium in grey (based on the GFP channel). (a) Example of merging of two small meshes, marked by arrows (yellow and light blue). Scale bar: 5 μm. i to v: illustration of the proposed mechanism based on the 3D reconstructions above (b) Example of a growing mesh (blue arrow) and a reversible mesh merging (yellow and magenta arrows). Note the increasing diameter of the mesh marked with the blue arrow between time point 37:50 and 40:10 and again at 46:20. The two meshes marked with a yellow and a magenta arrow fuse at time point 37:50 and separate again at 40:10. Scale bars: 20 μm. (c, d) Disappearance of several pillars in one region by merging with meshes. The pillar marked with a yellow arrow fuses with the mesh on the bottom left of the image (blue arrow) between time point 44:10 and 46:20. The other pillar, marked with a light blue arrow, fuses with another mesh between time point 43:40 and 44:10. Unlike merging of meshes, the fusion of a pillar with a nearby structure is not accompanied by a visible increase in its size. The 3D reconstruction was done only from the area within the white rectangle. Time points (hh:mm post fertilisation) are valid for each column. Scale bar: 5 μm. i to v: illustration of the proposed mechanism of the 3D reconstructions above.

A further mechanism of pillar disappearance was thinning and subsequent rupture (n=9, Figure 7, cyan arrow). It began with elongation of the pillar, rupture of its core, and then rapid thinning and rupture of the pillar envelope too. In contrast to our expectation, we did not observe appearance of new serried pillars at the branching points, and expected vessel splitting by merging of serried pillars (or small meshes) often did not take place (Figure 7 (d)).

Plexus remodelling was driven by the behaviour of meshes, namely their merging (Figure 7 (a)) or less frequently their fragmentation (Figure 7 (b)), and their growth (as described above and Figure 7 (b)). Most of the meshes tracked back from 48 hpf were present already at 28 hpf, the new ones formed usually by sprouting angiogenesis at the growing front of the plexus or less frequently by fragmentation of a mesh.

The first step in merging of meshes seemed to be the reduction of the flow in the connecting branch between the two meshes. As the flow ceased and eventually stopped, the lumen of the connecting branch closed like a camera aperture (as if the pressure that held it expanded disappeared and the tube now relaxed) (Figure 7 (a)). The opening in the lumen closed and eventually disappeared, and then the endothelial cells that had formed this connection retracted away, similarly to the process named “vascular pruning”.

Splitting of an existing mesh was occasionally seen in very narrow ones, where the two opposite branches eventually touched each other and got connected (Figure 7 (b). Splitting and merging was often reversible, as documented in the selected example.

2.6. Plexus simplification and establishment of hierarchy

The major events in plexus remodelling were arteriovenous or venous splitting (Figure 8) that occurred by the fusion of neighbouring meshes. As the plexus expanded caudally, numerous meshes formed in the distal part. The onset of circulation is around 24-26 hpf, and around 28-32 hpf there were numerous connections between the dorsal artery and the venous plexus. The less used ones located most cranially began to close first. Simultaneously, the plexus continued to grow, the lumen gradually opened in the caudal branches, and meshes located there expanded and fused with each other too. Around 48 hpf, the dorsal aorta usually drained to the venous plexus via one or a few branches.

Preprints (www.preprints.org) | NOT PEER-REVIEWED | Posted: 31 August 2023 doi:10.20944/preprints202308.2080.v1

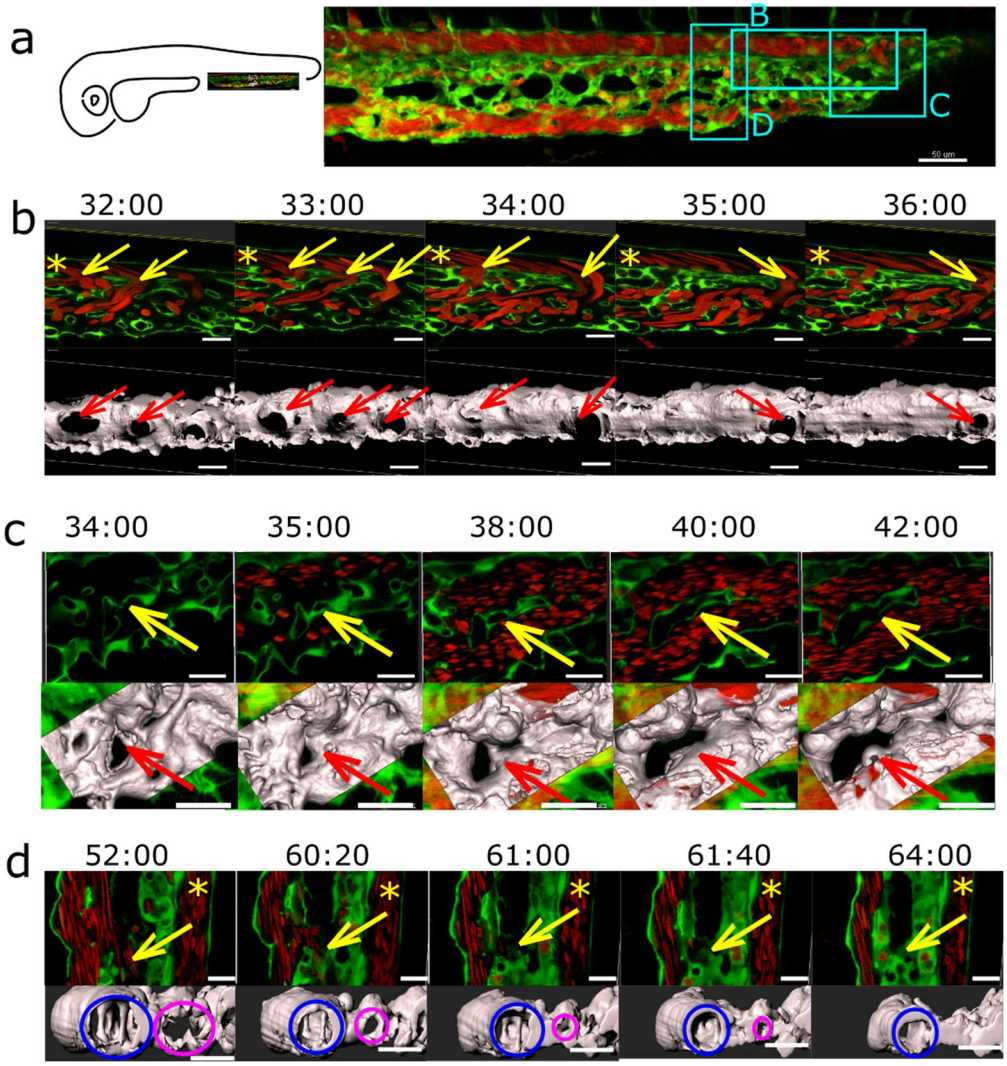

Figure 8. Arteriovenous and venous splitting. (a): Overview of the CVP of Fli1a:eGFP//Gata1:dsRed embryos showing the region where image sequences b-d were taken (since these were from different embryos, this is just a typical example CVP). DA marked with an asterisk. Endothelium in green, erythrocytes in red, 3D reconstruction in grey (based on the eGFP channel). (b): Arteriovenous splitting. The image sequence shows connections between the DA and the CV marked with yellow arrows that gradually close except for the most caudal one: thus, the blood flow shifts towards the caudal end of the plexus. First row: single slice. Second row: 3D reconstruction, showing the arteriovenous connections (red arrows). (c): Venous splitting at the growing front of the plexus occurs by merging of meshes. First row: single slice. Second row: 3D reconstruction within the rectangle in grey. (d): (Intussusceptive) Arborisation: The lumen of a redundant venous segment (magenta circle) in the central part of the CVP gradually shrinks and eventually fully collapses, leaving only the lumen of the caudal vein (blue circle) patent. First row: single slice. Second row: 3D reconstruction in grey. Time points (hh:mm post fertilisation) are valid for both columns, respectively. Scale bars: in a: 50 µm, b-d: 20 µm.

The closure of the redundant connections between DA and veins went along with a reduction of flow through them, but since the arteriovenous splitting took part in sih embryos too [data not shown], we suggest that this happened rather due to blood flow differences or a gradient than due to the absolute values.

Venous splitting was not so well predictable but followed the same principle. It took place at the onset of perfusion in the peripheral parts of the plexus (Figure 8 (c)), or as flow conditions changed (Figure 8 (b)). However, although the venous flow was almost exclusively restricted to the most

 doi:10.20944/preprints202308.2080.v1

ventral branch of the venous plexus, most meshes in the central part of the plexus didn't merge with each other by 2.5-3 dpf. Merging of the meshes was not solely responsible for the establishment of hierarchy between small and big veins.

Redirection of the flow through the most ventral vessel (the caudal vein) occured by lumen collapse or even closure of the segments forming the central part of the plexus. As the blood flow through the central part of the plexus dropped between 2-3 dpf, the lumens in the interconnecting segments gradually shrank and eventually collapsed (Figure 8 (d)). The lumen closure was not followed by endothelial cell retraction, as would be the case in pruning.

3. Discussion

The concept of intussusceptive angiogenesis was first presented in 1986. It describes the formation of pillars within the vessel lumen and their fusion, leading to vessel splitting and remodelling [42]. Since then, a big body of evidence has been collected on this phenomenon [43]. The morphology of intraluminal pillars and their existence in different vessel beds has been well documented, but the dynamic aspects of this process, namely how the pillars form in vivo and how they facilitate vessel splitting, remained largely unexplained. The availability of suitable transgenic models and the improvements of confocal microscopy in the recent years made such studies possible. We have used the zebrafish caudal vein plexus model that was established in our laboratory by Karthik et al. [8] and documented the formation of the transluminal pillars and their contribution to the plexus development in high spatio-temporal resolution.

Most pillars were present in the venous part of the CVP, and they were orientated perpendicular to the symmetry plane of the embryo, but one or a few pillars were usually present in the distal part of the dorsal aorta (oriented rather diagonally). Pillars were most numerous between 32-48 dpf, with a very high interindividual heterogeneity. There was a significant reduction in the pillar number from 3 dpf onwards, although some of the pillars persisted until at least 4 dpf. These data correlate with previous findings in our group [8]. We measured an average pillar diameter of 1.7±0.7 μm and an average length of 11±4.5 μm, and their ultrastructure corresponded to the intussusceptive pillars documented before [data not shown].

A problem in comparing our results with other studies is the paucity of quantitative data on pillar dimensions and the inconsistency of literature regarding the definition of a pillar. Most studies defined a pillar as a cylindrical structure with a diameter of 1-2.5 μm seen on SEM or on serial TEM sections, some extended the cut-off to up to 4 μm [44] or did not specify a cut-off at all. Foehst et al. developed an automated algorithm that classified all transluminal columns of a given diameter (they decided on 1 - 5 μm) [45], and they reported a highly asymmetric distribution of pillar diameter and volumes, with most pillars being between 1-3 μm in diameter and having a volume of less than 40 μm^3 (our average measurements of diameter and length would correspond to a volume of 25 μm^3). In order to see if the (most cited) cut-off at 2.5 μm was appropriate, we included in our quantifications (diameter and height, Figure 2, and area change, Figure 7) structures up to 4 μm (or up to 12 μm^2 in cross-section). The majority of pillars were indeed in the range of 1-2.5 μm and had the typical cylindrical shape.

Among the 74 pillars that were tracked back to their formation, we observed three processes involved in pillar formation: sprouting (formation of filopodia that "embrace" the future pillar core), lumen formation/expansion, and formation of a fold in an already lumenised vessel (capillary wall folding). This does not mean that there were three distinct mechanisms, it was rather a highly heterogeneous process where these three events participated to a certain degree, possibly depending on how mature the vasculature was at the time of pillar formation. Pillar formation by capillary wall folding has already been proposed before by Patan et al. [18] based on TEM data. We could identify vertical tissue folds and intermediates that they termed "pre-pillars" as immediate predecessors of the pillars that we observed by confocal microscopy. According to Patan et al., the pre-pillars formed in already lumenised vessels after the sprouting had ceased. Our data indicated that they may also appear earlier, during lumen formation, and have their origin in sprouting angiogenesis. We also observed thin intraluminal connections reminiscent of endothelial bridges described by Paku et al.

[19], but their nature was more transient, and they seemed to have no particular function. Contrary to our expectations, none of the observed thin transluminal pillars did form by the intraluminal invagination and perfusion of the contact zone.

Pillar formation is thought to occur preferably at branching points of vessels, triggered by a local drop of shear stress [12]. We used *sih* embryos (bearing a mutation in cardiac troponin and thus totally lacking blood flow) to test whether the pillar formation was flow dependent. Our results showed an impairment of mesh formation as reported previously by Xie et al. [41], but pillars were present nonetheless and their formation resembled the mechanisms described in the wt embryos. The insertion of pillars in the CVP of *sih*-embryos was therefore, contrary to previous findings [4, 8], not driven by local differences in blood flow or shear stress. An important remark here is that the computer models of flow-dependent pillar insertion were built on the intraluminal capillary wall fusion mechanism, which we did not confirm in the developing CVP. Yet another point might be that the in silico calculations [12] and in vivo data showing dependence of pillar formation on the blood flow referred to structures of 5-10 μm as "pillars" [8]. The formation of structures of this diameter (termed "meshes" in our work) was according to our data indeed impaired under no flow conditions.

The concept of intussusception postulates that intercapillary meshes evolve from transluminal pillars that increase their diameter as they get penetrated by perivascular cells (e.g. myofibroblasts or pericytes [1,20,46]). To examine this hypothesis, we tracked back meshes in time. Between 28-48 hpf, there were some newly formed meshes (by SA) or pillars, and there were some cases of mesh merging or splitting, but the majority of structures only changed their size. While the majority of meshes grew (39/62 grew by more than +50%), the majority of pillars (or very small meshes: cross-sectional area below 12 μm2 or below 4 μm in diameter) did not change much or shrank (only 1/17 changed their area by more than +50%, namely by +209%). This growing structure originally had a diameter of 3.5 μm: without information about the ultrastructure, we cannot tell with certainty whether this was a true case of pillar growth or whether, which we tend to believe, this was a tiny mesh already from the beginning.

The intercapillary meshes were thus, contrary to our expectations, not a later stage of intussusceptive pillars, but formed by SA ([22,47]). These meshes were highly dynamic and effectively shaped the vascular bed in the later stages of plexus remodelling and simplification. Pillars usually persisted in the lumen for several hours without any change in diameter or shape, and many eventually disappeared by rupture or fused back with the vessel wall ("capillary wall folding" reversed). The average lifetime of the observed pillars cannot be calculated since our 14 - 16-hour long scans contained only a few cases of the complete life of a pillar. A possible reason for the observed lack of growth of slender pillars might be a strong interaction between endothelial cell receptors and ECM constituents of the pillar core [48], that simply do not allow infiltration of pillars by perivascular cells. In contrast, small meshes might have a core consisting of diverse ECM components and cell extensions that is less dense and thus more plastic.

The question, how the interplay between SA and IA might be, is difficult to answer since it depends on (1) how we define intussusception or a pillar as the hallmark of IA, (2) how we define a mesh or what is our hallmark of SA, (3) the methodology used and its limitations, and finally, (4) differences in physiology of the different models used.

The involvement of SA during the early development of the CVP, followed by the appearance of pillars at 36-48 dpf in our study correlates with previous findings ([8,22]). Our data also remind of the recently proposed piecemeal mechanism that integrates IA and SA [49]. They described it as a combination of sprouting and intussusception angiogenesis, where sprouting stands at the beginning of the process and the appearance of pillars/papillae shows intussusception to be part of the following process.

So, how can we integrate the findings of our study into the broader picture of earlier research in this field? If intussusception is defined as the in-itself folding of a vessel leading to an insertion of intraluminal pillars, then we found no support of this mechanism. If we leave the mechanism aside and focus on insertion of pillars and their expansion into bigger intercapillary meshes, then we also found little evidence supporting this concept. The dynamics of pillar count per CVP we observed

recapitulated the data of Karthik et al. [8], but the slender pillars did not grow and the development of the CVP was dominated by the behaviour of meshes that arose by SA.

On the other hand, if intussusception is defined according to the outcomes, then the initial increase of plexus complexity resembled the IMG described in earlier studies about IA [21]. In line with the concept of IMG, the increase of vessel surface area did not appear to be attributable to endothelial cell proliferation, but rather by migration and flattening of endothelial cells (qualitative observations, data not shown). However, unlike in IMG, we did not observe growth of pillars (<2.5 µm in diameter). Furthermore, the later CVP development followed the pattern described as IAR. The growth and merging of intercapillary spaces served to split vessels, and changes in lumen diameter further established the hierarchy. The third possible outcome of intussusception, namely pillar formation being involved in branching point remodelling as proposed in IBR, has not been observed in CVP. We rather observed pillar disappearance (by rupture or by fusion with the vessel wall), not their formation, in response to changed flow condition.

The pillar formation and its further fate might depend on the chosen model. Chicken chorioallantoic membrane, mouse retina, capillary networks in the developing lung or kidney or in solid tumours might rather expand "within themselves", whereas the CVP of zebrafish rather expands its borders. Alternatively, the behaviour of pillars in the CVP might be specific for lower vertebrates - which is in our opinion rather unlikely, since the homology between fish and mammalian genes is generally high. All this would require further investigation.

To summarize, our data demonstrated that, when discriminating IA from SA, it is important to distinguish between the thin intussusceptive pillars and the bigger intercapillary meshes. Firstly, pillars and small meshes differ in their shape and their content. Secondly, according to our findings, pillars and small meshes have different mechanisms of formation, the latter originating by sprouting angiogenesis and not by the growth of small pillars. In contrast, the formation of pillars seemed to be driven by three major processes, which we described earlier. Thirdly, they behave differently – possibly since they have a different content. This also means that they have different roles or a different fate in the developing plexus.

4. Materials and Methods

4.1. Animals

Zebrafish (Danio rerio) were originally obtained from the Zebrafish International Resource Center (https://zebrafish.org/home/guide.php). They were maintained at standard conditions in a conventional fish facility at the Institute of Anatomy of the University of Bern. Embryos were raised in an incubator in petri dishes with E3 medium at 28.5°C and staged by hpf. The following zebrafish lines were used in this study: *Tg(fli1a :eGFP)y7* [50], *Tg(gata1: DsRed)sd2* [51], and *sih* (bearing a mutation in *tnnt2a* , a gene encoding cardiac troponin T) [52]. The choice of these transgenic lines was made in order to be able to study the development of the endothelium and the blood flow. The silent heart embryos, due to the missing blood circulation, enabled us to document the CVP formation without shear stress.

For live microscopy, embryos were manually dechorionated at 24 hpf and mounted from 28hpf in glass-bottom Petri dishes in E3 medium containing 0.167% low-melting agarose, 0.0175% tricaine and 72 µM phenylthiourea (all from Sigma-Aldrich, https://www.sigmaaldrich.com.) [21].

4.2. Live Imaging

Confocal scans of the developing CVP were acquired with a Zeiss LSM880 microscope, objective: 40x/1.1 LD-C-Apochromat W (https://www.zeiss.com), in a heated and humidified chamber (28.5°C) with a resolution of 0.16-0.35 µm in xy, 0.5-0.75 µm in z, and a time step of 10 min. The time point format hh:mm refers to the age of embryo in hours and minutes post fertilisation. Mounting and prolonged imaging (10h+) resulted in small deformations of the tail and a slight reduction of the body size and blood velocity (compare [21]), but no other signs of distress and no phototoxicity were observed and the patterns of the CVP were indistinguishable from freely hatched siblings. Analyses

of pillar morphology, pillar formation, development, mesh dynamics, and the quantification of the area change are based on 6 confocal scans starting between 28 - 32 hpf and ending at 44 - 48 hpf. Pillar count per plexus was based on 11-28 replicates per time point.

4.3. Pillar tracking

A sub-volume of the total image size between 50x50x17 µm and 100x100x26 µm around each pillar was tracked in 3D over time on the full-size time-lapse image dataset, using software developed by Vladymyrov [53]. This software was initially designed to perform correction of the tissue drift in real-time during in vivo acquisitions [24]. Its core is an algorithm performing fine pattern matching in 3D, which can be applied to a number of tracking tasks. A function to perform tracking of 3D sub-volumes was developed especially for this project. In addition, since the tissue shape was changing quickly during the development of the embryo, the alignment timeframe had to be reduced from 30 timeframes to 1 timeframe. This allowed for keeping high correlation values in the offsets probability map and enabled robust tracking of the region of interest. The tracking procedure output was a list of the pillar coordinates at each time point in the original dataset and a set of 3D image crops around this position. Those image crops were used for further visual inspection. Since the xyz coordinates of the pillars shifted as the plexus grew, scans had to be processed so that the pillars were centred in a defined region of interest at each time point.

4.4. Image analysis, Statistics, Artwork

Measurements and analyses were done manually using Fiji, the diameter and cross-section areas were measured at 44-48hpf in the middle of the pillar, the accuracy of the length/height measurements was 0.5 µm and the cross-section areas were rounded to full µm². 3D representations of endothelial surface were created in Imaris. Graphs were generated using Stata (also used for statistics) or Excel software, illustrations were created in Inkscape and MediBang Paint Pro. Data such as pillar length, height, pillar count per plexus per time point are given as mean ± standard deviation.

5. Conclusions

We brought evidence that a) transluminal pillars in the CVP formed by different mechanisms than the classical intussusception, b) their formation was independent of the blood flow, and c) the thin pillars did not get thicker with time as expected but rather stayed the same or even shrank and disappeared, and d) plexus remodelling was driven by the dynamics of bigger intercapillary meshes, not pillars. Further experiments are needed to decipher the pillar formation in mammalian vascular beds, and to investigate whether they contribute to plexus remodelling. We showed that clear unambiguous criteria are needed to discriminate between IA and SA, and we strongly suggest that evidence is based on time-lapse 3D data.

Supplementary Materials: The following supporting information can be downloaded at the website of this paper posted on Preprints.org. Suppl. Fig. S1: Formation of a pillar and subsequent rupture; Suppl. Fig. S2: Formation of a pillar and its disappearance by merging with the vessel wall.; Suppl. Fig. S3: Formation of a pillar by sprouting angiogenesis.; Suppl. Fig. S4: Pillar behaviour.

Author Contributions: Conceptualization, V.D.; methodology, H.R.; software, M.V.; validation, M.V. and H.R.; investigation and data analysis, H.R., A.O. and D.A.; writing, H.R. and D.A.; visualization, H.R.; supervision, V.D.; funding acquisition, V.D. All authors have read and agreed to the published version of the manuscript.

Funding: This research was funded by the Swiss Cancer Research foundation (KFS-4281-08-2017) and the Swiss National Science Foundation (SNSF 31003A_176038/1).

Institutional Review Board Statement: The animal experiments performed in this study conformed to the guidelines of the Swiss government and were prospectively approved by the Bernese cantonal veterinary office under the licenses BE59/15 and BE45/19. There is no Institutional Animal Care and Use Committee (IACUC) that pre-approves experiments at the University of Bern or other relevant ethics board needed for our experiments.

Data Availability Statement: Not applicable.

Acknowledgments: We would like to thank the following people: Cristian Fernandez Palomo for proofreading and inputs on the manuscript; Marco Röss for the illustrations of the observed processes.

Conflicts of Interest: The authors declare that there is no conflict of interest. The funders had no role in the design of the study; in the collection, analysis, or interpretation of data; in the writing of the manuscript; or in the decision to publish the results.

References

1. Burri, P.H.; Djonov, V. Intussusceptive angiogenesis—the alternative to capillary sprouting. *Mol. Aspects Med.* **2002**, *23*, 1–27, doi:10.1016/S0098-2997(02)00096-1.
2. Schlatter, P.; König, M.F.; Karlsson, L.M.; Burri, P.H. Quantitative Study of Intussusceptive Capillary Growth in the Chorioallantoic Membrane (CAM) of the Chicken Embryo. *Microvasc. Res.* **1997**, *54*, 65–73, doi:10.1006/mvre.1997.2022.
3. Djonov, V.G.; Galli, A.B.; Burri, P.H. Intussusceptive arborization contributes to vascular tree formation in the chick chorio-allantoic membrane. *Anat. Embryol. (Berl.)* **2000**, *202*, 347–357, doi:10.1007/s004290000126.
4. Djonov, V.G.; Kurz, H.; Burri, P.H. Optimality in the developing vascular system: Branching remodeling by means of intussusception as an efficient adaptation mechanism. *Dev. Dyn.* **2002**, *224*, 391–402, doi:10.1002/dvdy.10119.
5. Patan, S. TIE1 and TIE2 Receptor Tyrosine Kinases Inversely Regulate Embryonic Angiogenesis by the Mechanism of Intussusceptive Microvascular Growth. *Microvasc. Res.* **1998**, *56*, 1–21, doi:10.1006/mvre.1998.2081.
6. Gorczyca, J.; Litwin, J.A.; Nowogrodzka-Zagórska, M.; Skawina, A.; Miodoński, A.J. Architecture of blood vessels in human fetal gastric corpus: a corrosion casting study. *Ann. Anat. - Anat. Anz.* **1999**, *181*, 353–358, doi:10.1016/S0940-9602(99)80127-7.
7. Lametschwandtner, A.; Lametschwandtner, U.; Radner, Ch.; Minnich, B. Spatial growth and pattern formation in the small intestine microvascular bed from larval to adult Xenopus laevis: a scanning electron microscope study of microvascular corrosion casts. *Anat. Embryol. (Berl.)* **2006**, *211*, 535–547, doi:10.1007/s00429-006-0104-2.
8. Karthik, S.; Djukic, T.; Kim, J.-D.; Zuber, B.; Makanya, A.; Odriozola, A.; Hlushchuk, R.; Filipovic, N.; Jin, S.W.; Djonov, V. Synergistic interaction of sprouting and intussusceptive angiogenesis during zebrafish caudal vein plexus development. *Sci. Rep.* **2018**, *8*, 9840, doi:10.1038/s41598-018-27791-6.
9. Djonov, V.; Baum, O.; Burri, P.H. Vascular remodeling by intussusceptive angiogenesis. *Cell Tissue Res.* **2003**, *314*, 107–117, doi:10.1007/s00441-003-0784-3.
10. Polykandriotis, E.; Euler, S.; Arkudas, A.; Pryymachuk, G.; Beier, J.P.; Greil, P.; Dragu, A.; Lametschwandtner, A.; Kneser, U.; Horch, R.E. Regression and persistence: remodelling in a tissue engineered axial vascular assembly. *J. Cell. Mol. Med.* **2009**, *13*, 4166–4175, doi:10.1111/j.1582-4934.2009.00828.x.
11. Szczerba, D.; Székely, G. A Computational Model of Micro-vascular Growth. In *Computational Science – ICCS 2005*; Sunderam, V.S., van Albada, G.D., Sloot, P.M.A., Dongarra, J., Eds.; Lecture Notes in Computer Science; Springer Berlin Heidelberg: Berlin, Heidelberg, 2005; Vol. 3516, pp. 17–24 ISBN 978-3-540-26044-8.
12. Filipovic, N.; Tsuda, A.; Lee, G.S.; Miele, L.F.; Lin, M.; Konerding, M.A.; Mentzer, S.J. Computational flow dynamics in a geometric model of intussusceptive angiogenesis. *Microvasc. Res.* **2009**, *78*, 286–293, doi:10.1016/j.mvr.2009.08.004.
13. Mentzer, S.J.; Konerding, M.A. Intussusceptive angiogenesis: expansion and remodeling of microvascular networks. *Angiogenesis* **2014**, *17*, 499–509, doi:10.1007/s10456-014-9428-3.
14. Styp-Rekowska, B.; Hlushchuk, R.; Pries, A.R.; Djonov, V. Intussusceptive angiogenesis: pillars against the blood flow: Intussusception and biomechanical forces. *Acta Physiol.* **2011**, *202*, 213–223, doi:10.1111/j.1748-1716.2011.02321.x.
15. Makanya, A.N.; Stauffer, D.; Ribatti, D.; Burri, P.H.; Djonov, V. Microvascular growth, development, and remodeling in the embryonic avian kidney: The interplay between sprouting and intussusceptive angiogenic mechanisms. *Microsc. Res. Tech.* **2005**, *66*, 275–288, doi:10.1002/jemt.20169.
16. Ribatti, D.; Crivellato, E. "Sprouting angiogenesis", a reappraisal. *Dev. Biol.* **2012**, *372*, 157–165, doi:10.1016/j.ydbio.2012.09.018.
17. Patan, S.; Haenni, B.; Burri, P.H. Implementation of Intussusceptive Microvascular Growth in the Chicken Chorioallantoic Membrane (CAM): 2. Pillar Formation by Capillary Fusion. *Microvasc. Res.* **1997**, *53*, 33–52, doi:10.1006/mvre.1996.1989.
18. Patan, S.; Haenni, B.; Burri, P.H. Implementation of Intussusceptive Microvascular Growth in the Chicken Chorioallantoic Membrane (CAM): 1. pillar formation by folding of the capillary wall. *Microvasc. Res.* **1996**, *51*, 80–98, doi:10.1006/mvre.1996.0009.

19. Paku, S.; Dezső, K.; Bugyik, E.; Tóvári, J.; Tímár, J.; Nagy, P.; Laszlo, V.; Klepetko, W.; Döme, B. A New Mechanism for Pillar Formation during Tumor-Induced Intussusceptive Angiogenesis: Inverse Sprouting. *Am. J. Pathol.* **2011**, *179*, 1573–1585, doi:10.1016/j.ajpath.2011.05.033.
20. Djonov, V.; Schmid, M.; Tschanz, S.A.; Burri, P.H. Intussusceptive angiogenesis: its role in embryonic vascular network formation. *Circ. Res.* **2000**, *86*, 286–292, doi:10.1161/01.res.86.3.286.
21. Kaufmann, A.; Mickoleit, M.; Weber, M.; Huisken, J. Multilayer mounting enables long-term imaging of zebrafish development in a light sheet microscope. *Dev. Camb. Engl.* **2012**, *139*, 3242–3247, doi:10.1242/dev.082586.
22. Wiley, D.M.; Kim, J.-D.; Hao, J.; Hong, C.C.; Bautch, V.L.; Jin, S.-W. Distinct signalling pathways regulate sprouting angiogenesis from the dorsal aorta and the axial vein. *Nat. Cell Biol.* **2011**, *13*, 686–692, doi:10.1038/ncb2232.
23. Murayama, E.; Kissa, K.; Zapata, A.; Mordelet, E.; Briolat, V.; Lin, H.-F.; Handin, R.I.; Herbomel, P. Tracing hematopoietic precursor migration to successive hematopoietic organs during zebrafish development. *Immunity* **2006**, *25*, 963–975, doi:10.1016/j.immuni.2006.10.015.
24. Isogai, S.; Horiguchi, M.; Weinstein, B.M. The vascular anatomy of the developing zebrafish: an atlas of embryonic and early larval development. *Dev. Biol.* **2001**, *230*, 278–301, doi:10.1006/dbio.2000.9995.
25. De Spiegelaere, W.; Casteleyn, C.; Van den Broeck, W.; Plendl, J.; Bahramsoltani, M.; Simoens, P.; Djonov, V.; Cornillie, P. Intussusceptive Angiogenesis: A Biologically Relevant Form of Angiogenesis. *J. Vasc. Res.* **2012**, *49*, 390–404, doi:10.1159/000338278.
26. Chouinard-Pelletier, G.; Jahnsen, E.D.; Jones, E.A.V. Increased shear stress inhibits angiogenesis in veins and not arteries during vascular development. *Angiogenesis* **2013**, *16*, 71–83, doi:10.1007/s10456-012-9300-2.
27. Baum, O.; Suter, F.; Gerber, B.; Tschanz, S.; Buergy, R.; Blank, F.; Hlushchuk, R.; Djonov, V. VEGF-A Promotes Intussusceptive Angiogenesis in the Developing Chicken Chorioallantoic Membrane. *Microcirc. N. Y. N 1994* **2010**, *17*, 447–457, doi:10.1111/j.1549-8719.2010.00043.x.
28. Ackermann, M.; Kim, Y.O.; Wagner, W.L.; Schuppan, D.; Valenzuela, C.D.; Mentzer, S.J.; Kreuz, S.; Stiller, D.; Wollin, L.; Konerding, M.A. Effects of nintedanib on the microvascular architecture in a lung fibrosis model. *Angiogenesis* **2017**, *20*, 359–372, doi:10.1007/s10456-017-9543-z.
29. Polykandriotis, E.; Arkudas, A.; Beier, J.; Dragu, A.; Rath, S.N.; Pryymachuk, G.; Schmidt, V.; Lametschwandtner, A.; Horch, R.; Kneser, U. The impact of VEGF and bFGF on vascular stereomorphology in the context of angiogenic neo-arborisation after vascular induction. *J. Electron Microsc. (Tokyo)* **2011**, *60*, 267–274, doi:10.1093/jmicro/dfr025.
30. Mukwaya, A.; Peebo, B.; Xeroudaki, M.; Ali, Z.; Lennikov, A.; Jensen, L.; Lagali, N. Factors regulating capillary remodeling in a reversible model of inflammatory corneal angiogenesis. *Sci. Rep.* **2016**, *6*, 32137, doi:10.1038/srep32137.
31. Bugyik, E.; Dezső, K.; Reiniger, L.; László, V.; Tóvári, J.; Tímár, J.; Nagy, P.; Klepetko, W.; Döme, B.; Paku, S. Lack of Angiogenesis in Experimental Brain Metastases. *J. Neuropathol. Exp. Neurol.* **2011**, *70*, 979–991, doi:10.1097/NEN.0b013e318233afd7.
32. Sarı Kılıçaslan, S.M.; Coşkun Cevher, Ş.; Güleç Peker, E.G. Ultrastructural changes in blood vessels in epidermal growth factor treated experimental cutaneous wound model. *Pathol. - Res. Pract.* **2013**, *209*, 710–715, doi:10.1016/j.prp.2013.08.005.
33. Giacomini, A.; Ackermann, M.; Belleri, M.; Coltrini, D.; Nico, B.; Ribatti, D.; Konerding, M.A.; Presta, M.; Righi, M. Brain angioarchitecture and intussusceptive microvascular growth in a murine model of Krabbe disease. *Angiogenesis* **2015**, *18*, 499–510, doi:10.1007/s10456-015-9481-6.
34. Ceauşu, R.A.; Cîmpean, A.M.; Gaje, P.; Gurzu, S.; Jung, I.; Raica, M. CD105/Ki67 double immunostaining expression in liver metastasis from colon carcinoma. *Romanian J. Morphol. Embryol. Rev. Roum. Morphol. Embryol.* **2011**, *52*, 613–616.
35. Bai, L.; Wu, D.; Xu, J.; Liu, H.; Xie, M.; Guan, G.; Sun, Z.; Tan, X. On model of angiogenesis and the mechanism in porous silk fibroin films. *J. Mater. Sci. Mater. Med.* **2011**, *22*, 927–933, doi:10.1007/s10856-011-4258-y.
36. Dimova, I.; Hlushchuk, R.; Makanya, A.; Styp-Rekowska, B.; Ceauşu, R.; Flueckiger, S.; Lang, S.; Semela, D.; Noble, F.; Chatterjee, S.; et al. Inhibition of Notch signaling induces extensive intussusceptive neo-angiogenesis by recruitment of mononuclear cells. *Angiogenesis* **2013**, *16*, doi:10.1007/s10456-013-9366-5.
37. Ackermann, M.; Morse, B.A.; Delventhal, V.; Carvajal, I.M.; Konerding, M.A. Anti-VEGFR2 and anti-IGF-1R-Adnectins inhibit Ewing's sarcoma A673-xenograft growth and normalize tumor vascular architecture. *Angiogenesis* **2012**, *15*, 685–695, doi:10.1007/s10456-012-9294-9.
38. Dill, M.T.; Rothweiler, S.; Djonov, V.; Hlushchuk, R.; Tornillo, L.; Terracciano, L.; Meili–Butz, S.; Radtke, F.; Heim, M.H.; Semela, D. Disruption of Notch1 Induces Vascular Remodeling, Intussusceptive Angiogenesis, and Angiosarcomas in Livers of Mice. *Gastroenterology* **2012**, *142*, 967-977.e2, doi:10.1053/j.gastro.2011.12.052.

39. Rossi-Schneider, T.; Verli, F.; Marinho, S.; Yurgel, L.; Souza, M. Study of Intussusceptive Angiogenesis in Inflammatory Regional Lymph Nodes by Scanning Electron Microscopy. *Microsc. Res. Tech.* **2009**, *73*, 14–19, doi:10.1002/jemt.20747.
40. Phng, L.-K.; Belting, H.-G. Endothelial cell mechanics and blood flow forces in vascular morphogenesis. *Semin. Cell Dev. Biol.* **2021**, *120*, 32–43, doi:10.1016/j.semcdb.2021.06.005.
41. Xie, X.; Zhou, T.; Wang, Y.; Chen, H.; Lei, D.; Huang, L.; Wang, Y.; Jin, X.; Sun, T.; Tan, J.; et al. Blood Flow Regulates Zebrafish Caudal Vein Plexus Angiogenesis by ERK5-klf2a-nos2b Signaling. *Curr. Mol. Med.* **2018**, *18*, 3–14, doi:10.2174/1566524018666180322153432.
42. Caduff, J.H.; Fischer, L.C.; Burri, P.H. Scanning electron microscope study of the developing microvasculature in the postnatal rat lung. *Anat. Rec.* **1986**, *216*, 154–164, doi:10.1002/ar.1092160207.
43. Du Cheyne, C.; Smeets, M.; De Spiegelaere, W. Techniques used to assess intussusceptive angiogenesis: A systematic review. *Dev. Dyn.* **2021**, *250*, 1704–1716, doi:10.1002/dvdy.382.
44. Konerding, M.A.; Gibney, B.C.; Houdek, J.P.; Chamoto, K.; Ackermann, M.; Lee, G.S.; Lin, M.; Tsuda, A.; Mentzer, S.J. Spatial dependence of alveolar angiogenesis in post-pneumonectomy lung growth. *Angiogenesis* **2012**, *15*, 23–32, doi:10.1007/s10456-011-9236-y.
45. Föhst, S.; Wagner, W.; Ackermann, M.; Redenbach, C.; Schladitz, K.; Wirjadi, O.; Ysasi, A.B.; Mentzer, S.J.; Konerding, M.A. Three-dimensional image analytical detection of intussusceptive pillars in murine lung. *J. Microsc.* **2015**, *260*, 326–337, doi:10.1111/jmi.12300.
46. Burri, P.H.; Hlushchuk, R.; Djonov, V. Intussusceptive angiogenesis: Its emergence, its characteristics, and its significance. *Dev. Dyn.* **2004**, *231*, 474–488, doi:10.1002/dvdy.20184.
47. Wakayama, Y.; Fukuhara, S.; Ando, K.; Matsuda, M.; Mochizuki, N. Cdc42 Mediates Bmp-Induced Sprouting Angiogenesis through Fmnl3-Driven Assembly of Endothelial Filopodia in Zebrafish. *Dev. Cell* **2015**, *32*, 109–122, doi:10.1016/j.devcel.2014.11.024.
48. Davis, G.E.; Senger, D.R. Endothelial extracellular matrix: biosynthesis, remodeling, and functions during vascular morphogenesis and neovessel stabilization. *Circ. Res.* **2005**, *97*, 1093–1107, doi:10.1161/01.RES.0000191547.64391.e3.
49. Díaz-Flores, L.; Gutiérrez, R.; García, M.D.P.; Sáez, F.J.; Díaz-Flores, L.; Madrid, J.F. Piecemeal Mechanism Combining Sprouting and Intussusceptive Angiogenesis in Intravenous Papillary Formation Induced by PGE2 and Glycerol. *Anat. Rec. Hoboken NJ 2007* **2017**, *300*, 1781–1792, doi:10.1002/ar.23599.
50. Lawson, N.D.; Weinstein, B.M. In vivo imaging of embryonic vascular development using transgenic zebrafish. *Dev. Biol.* **2002**, *248*, 307–318, doi:10.1006/dbio.2002.0711.
51. Traver, D.; Paw, B.H.; Poss, K.D.; Penberthy, W.T.; Lin, S.; Zon, L.I. Transplantation and in vivo imaging of multilineage engraftment in zebrafish bloodless mutants. *Nat. Immunol.* **2003**, *4*, 1238–1246, doi:10.1038/ni1007.
52. Sehnert, A.J.; Huq, A.; Weinstein, B.M.; Walker, C.; Fishman, M.; Stainier, D.Y.R. Cardiac troponin T is essential in sarcomere assembly and cardiac contractility. *Nat. Genet.* **2002**, *31*, 106–110, doi:10.1038/ng875.
53. Vladymyrov, M.; Abe, J.; Moalli, F.; Stein, J.V.; Ariga, A. Real-time tissue offset correction system for intravital multiphoton microscopy. *J. Immunol. Methods* **2016**, *438*, 35–41, doi:10.1016/j.jim.2016.08.004.